Tumor stage-driven disruption of NK cell maturation in human and murine lung tumors

Jules Russick, Carine Torset, Dan Sun, Solenne Marmier, Nicolas Merle, Elodie Voilin, Nathalie Josseaume, Maxime Meylan, Isaïas Hernandez, Pierre-Emmanuel Foy, et al.

Tumor stage-driven disruption of NK cell maturation in human and murine lung tumors

Jules Russick[1,2,3], Carine Torset[1,2,3], Dan Sun[4], Solenne Marmier[1,2,3], Nicolas Merle[1,2,3], Elodie Voilin[1,2,3], Nathalie Josseaume[1,2,3], Maxime Meylan[1,2,3], Isaïas Hernandez[1,2,3], Pierre-Emmanuel Foy[1,2,3], Pierre-Emmanuel Joubert[1,2,3], Marco Alifano[1,2,3,5], Audrey Lupo[1,2,3,5], Sophie Siberil[1,2,3], Niklas K Björkström[4], Diane Damotte[1,2,3,5], Isabelle Cremer[1,2,3,6*]

Affiliations

1. INSERM, UMR_S 1138, Centre de Recherche des Cordeliers, Team "Inflammation, Complement and Cancer", F-75006, Paris, France

2. Sorbonne Universite, Centre de Recherche des Cordeliers, F-75006, Paris, France

3. Universite Paris Cite, Centre de Recherche des Cordeliers, F-75006, Paris, France

4. Center for Infectious Medicine, Department of Medicine Huddinge, Karolinska Institute, Karolinska University Hospital, Stockholm, Sweden

5. Departments of Surgery and Pathology, Hopital Cochin Assistance Publique Hopitaux de Paris, F-75014 France

6. Lead contact

[*]**Correspondence** isabelle.cremer@sorbonne-universite.fr

Keywords

NK cells; lung cancer; tumor microenvironment; NK exclusion; NK dysfunction; single-cell sequencing; pseudotime; cytotoxicity; maturation.

Summary

Natural Killer (NK) cells play a pivotal role against cancer, both by direct killing of malignant cells and by promoting adaptive immune response though cytokine and chemokine secretion. In the lung tumor microenvironment (TME), NK cells are scarce and dysfunctional. By conducting single-cell transcriptomic analysis of lung tumors, and exploring pseudotime, we uncovered that the intratumoral maturation trajectory of NK cells is disrupted in a tumor stage-dependent manner, ultimately resulting in the selective exclusion of the cytotoxic subset. Using functional assays, we observed intratumoral NK cell death and a reduction in cytotoxic capacities depending on the tumor stage. Finally, our analyses of human public dataset on lung cancer corroborate these findings, revealing a parallel dysfunctional maturation process of NK cells during tumor progression. These results highlight additional mechanisms by which tumor cells escape from NK cell cytotoxicity, therefore paving the way for tailored therapeutic strategies.

Introduction

The tumor microenvironment (TME) of non-small-cell lung Cancer (NSCLC) is highly heterogeneous, complex, and dynamic[1] and comprises multiple immune cell types including innate immune cells. Natural killer (NK) cells are a heterogenous subset of cytotoxic innate lymphoid cells (ILCs) that express activating and inhibitory germline-encoded receptors. They exert two main functions: targeting and killing cancer cells, against which they represent the first line of defense[2], and secretion of immunomodulatory cytokines and chemokines[3,4], which in turn promotes intratumoral recruitment and activation of adaptive immune cells[5,6]. In human and mouse tissues, including lungs, distinct NK cell subsets have been described using single-cell transcriptomic analyses[7,8]. The maturation process of NK cells in mice has been well characterized. The genes that drive maturation and the phenotypic markers associated with different maturation stages have been identified[9,10]. Based on the expression of CD27 and CD11b markers, four NK cell maturation subsets exhibiting distinct functions, have been characterized: precursor ($CD27^-CD11b^-$), immature ($CD27^+CD11b^-$), mature ($CD27^+CD11b^+$), and fully mature ($CD27^-CD11b^+$)[11]. The most mature cells ($CD11b^+$) are the most cytotoxic, with strong degranulation and antibody-dependent cell cytotoxicity capacities, whereas the most immature cells ($CD27^+$) have been described as cytokine producers and are poorly cytotoxic[7,11–13].

In various solid tumor microenvironments, including lung cancer, NK cells are scarce compared to non-tumoral tissues. They also exhibit an altered phenotype, impaired cytotoxic function and reduced IFN-γ production, ultimately resulting in a compromised anti-tumor effect[5,14–20]. Mechanistically, it was demonstrated that NK cell dysfunction in KRAS-mutated lung tumors was due to a progressive aberrant expression of fructose-1,6-biphosphatase (FBP-1), which inhibits glycolysis and impairs NK cell viability[21]. The role of TGF-β secreted by tumor-

associated macrophages in impairing antitumor NK function has also been described in gastric carcinoma[22]. However, the impact of the TME on the infiltration and maturation processes of NK cell subsets during tumor progression remains unclear. Several hypotheses could account for the absence of functional NK cells in the TME, including potential defect in NK cell recruitment, impaired *in situ* maturation towards a cytotoxic phenotype, and/or specific killing of NK cells within the TME.

In this study, we initially demonstrated the progressive exclusion of NK cells from the TME during tumor progression. We conducted a comprehensive analysis of intratumoral NK cell heterogeneity using a single-cell transcriptomic approach, followed by a pseudotime analysis. Our findings revealed a profound impairment of the maturation process of NK cells within the murine and human TME, leading to a decrease in the population of cytotoxic NK cells. Furthermore, we observed an intratumoral NK cell death and a reduction in cytotoxic capacities depending on the tumor stage. These discoveries underscore a mechanism employed by tumor cells to evade NK cell lysis, involving the impairment of NK cell maturation towards cytotoxic NK cells.

Results

NK cell exclusion from the TME depends on the tumor progression

To evaluate the impact of tumor progression on NK cell phenotype and density within the TME, we used a murine orthotopic model of lung cancer, established through intratracheal injection of luciferase-expressing LLC cells (LLC-Luc). This model allows for precise and non-invasive monitoring of lung tumor progression using an *in vivo* imaging system (IVIS) (**Figure 1A**). The kinetics of tumor progression, quantified by the total flux representing photons emission per second (p/s), was highly heterogeneous (**Figure 1B**). We characterized the immune lymphoid infiltrates in the control and tumoral lungs using flow cytometry, with the gating strategy shown in **Figure S1A-B**. While the proportion of NK cells and $CD8^+$ T cells decreased in tumoral lungs compared to that in the control group, the proportions of $CD4^+$ T and B cells remained comparable across the two groups (**Figure 1C**). However, in the $CD4^+$ T cell compartment, we found an increased proportion of effector memory cells, and in the $CD8^+$ T cell compartment, we found an increased proportion of central and effector memory cells. To understand the dynamics of lymphoid population evolution during tumor progression, we correlated the proportion of each cell type with the tumor size. We found a significant negative correlation between tumor progression and the percentage of intratumoral NK cells, which was not observed in other cell types (**Figure 1D, Figure S1C**).

To delineate homogeneous groups based on tumor size in an unbiased manner, we plotted the difference between successive tumor sizes. We identified a gap between 317,800 and 431,300 p/s, indicating a threshold value distinguishing the two groups of tumors (**Figure S1D**). Tumors with a total flux $<4x10^5$ p/s were categorized as “small”, whereas those exceeding this threshold were designated as “large” tumors. This classification was validated at the tissue level after macro-dissection of the tumors, allowing visualization of non-tumoral areas and

small and large tumors in the lungs (**Figure S1E**), and hematoxylin and eosin staining (**Figure S1F**). Consequently, we confirmed the reduction in NK cell numbers in large versus small tumors and small tumors versus non-tumoral tissue, thereby confirming that NK cell exclusion is tumor size-dependent (**Figure 1E**). In all our analyses, the control group (mice injected with culture medium) and the non-tumoral group were similar, prompting us to consider adjacent non-tumoral samples as controls.

Subsequently, we compared the phenotype of NK cells in small and large tumors, focusing on markers previously identified in human lung tumors[19] (**Figure S2**). We observed a modification in the migration pattern of intratumoral NK cells, marked by a strong increased CXCR6 expression within the large tumor compared to non-tumoral lungs. Regarding the immune checkpoint molecules, less than 1 or 2% of NK cells expressed CTLA-4, PD-1, TIGIT and TIM-3. However, LAG-3 was strongly overexpressed in large tumors compared to non-tumoral tissues. Of note, NK cells in large tumors also showed increased cell surface CD107a degranulation marker expression, indicative of activated NK cells. Finally, to investigate the role of NK cells in controlling tumor growth, we initiated NK cell depletion at the onset of the tumor. Surprisingly, this did not affect tumor growth, suggesting that NK cells were very rapidly functionally unable to exert antitumor effects (**Figure 1F**).

Altogether, these results show that NK are largely excluded and altered during tumor progression, compromising their antitumor capacities.

Identification of cytotoxic and cytokine-producer subsets of intratumoral NK cells

To characterize NK cells more deeply, we conducted a single-cell transcriptomic experiment on cells isolated from both small and large tumors, comparing them to NK cells from adjacent non-tumoral tissues. Unsupervised clustering of NK cells from all groups generated a UMAP featuring 12 different clusters (clusters 0-11) (**Figure S3A**). Clusters 5, 9 and 10, corresponding

to contaminating B cells, macrophages and T cells, and expressing *Igkc*, *Cd68* and *Cd3e* genes, respectively, were excluded from further analyses (**Figure 2A, Figure S3B**). We then validated that the remaining cells were exclusively NK cells and did not comprise ILC2 cells, since they express *Klrb1c* (NK1.1)*, Ncr1* (NKp46)*, Klrk1 (NKG2D)*, and *Nkg7* (NKG7), but not *Il1rl1 (ST2),* which is expressed by ILC2 cells (**Figure S3C**). We compared the differentially expressed genes of all NK cells between the small and large tumors or non-tumoral tissues, using the MSigDB, GO and KEGG databases. We found that cytokine signaling and apoptosis pathways are the main pathways overexpressed in NK cells from large tumors compared to non-tumoral tissues or to small tumors **(Figure S3D)**. We thus decided to investigate the different NK cell profiles. Using the MAST method[23], we generated a heatmap showing the top 10 differentially expressed genes for each NK cell cluster compared to the others (**Figure 2B**). Subsequently, we identified the specific signature of each cluster and numerous genes related to cytotoxicity and cytokine production (**Table 1**). Enrichment analysis of differentially expressed transcripts confirmed their relevance to cytotoxicity-related pathways (ie. “NK cell mediated cytotoxicity”, “regulation of Natural Killer cell mediated cytotoxicity”, “positive regulation of Natural Killer cell mediated immunity”) and cytokine-related pathways (ie. “cytokine-cytokine receptor interaction”, “positive regulation of cytokine production”, “cytokine-mediated signaling pathway”). Consequently, we categorized clusters 0, 2 and 11 as “cytotoxic NK cells”, expressing high levels of cytotoxicity-related genes and low levels of cytokine regulation genes. Clusters 1, 3, 6, and 8 were designated as “cytokine-producing NK cells” (**Figure 2C**, **Figure S4A**). Assessment of *Itgam* (encoding CD11b) and *Cd27* gene expression confirmed the segregation between cytotoxic and cytokine-producing NK cell subsets (**Figure 3A**, **Figure S4B**). In accordance with Crinier *et al.*[7], cytotoxic clusters 0, 2 and 11 exhibited high levels of *Itgam*, *Gzmb*, *Prf1*, *Emp3*, *Itgb2*, *Zeb2*, *CybA and Cst7* transcripts, whereas cytokine-producing

clusters 1, 3, 6 and 8 expressed high levels of *Cd27*, *Xcl1* and *Ltb* (**Figure 3B**). Cluster 4, lacking a distinct functional profile, was characterized by strong expression of *Cxcr5*, while cluster 7 was identified as proliferative NK cells, showing high expression of *MiK67* (**Figure S3E**). The identification of distinct NK cell populations was then confirmed using MiloR and MiloDE packages, allowing a highly resolved differential gene expression analysis in a cluster-free manner[24,25] (**Figure S5)**. We then compared the gene expression profile of the Seurat-generated clusters and the Milo-generated nodes. To do so, we generated the DEGs between cytotoxic and cytokine-producer Seurat clusters (using the MAST method described in the manuscript) and Milo nodes (using "de_test_neighbourhoods" function). We compared both lists and found that 92.86% (13/14) of the genes found by Seurat were also found by MiloDE.

To evaluate the maturation dynamics of NK cells, we employed the Monocle 3 pseudotime algorithm, which computationally orders the transcriptomic profiles of cells along a trajectory without prior clustering information[26]. This analysis uncovered a developmental trajectory for NK cells, delineating a maturation path from cytokine-producing clusters to cytotoxic ones (**Figure 3C**). To validate this trajectory, we quantified the expression of genes known to be involved in the NK maturation process in mice (**Figure 3D, top**)[9,10,27]. Our findings indicate that genes associated with the early phase of maturation (prior to IL-15 sensitivity) exhibited comparatively higher expression levels before pseudotime=10, followed by a gradual decrease over pseudotime (**Figure 3D, bottom**). Conversely, genes associated with late-stage differentiation displayed a relative increase in expression levels throughout the pseudotime, reaching a maximum level at the latest pseudotime point (pseudotime=15 and onward). This confirmed the accuracy of the generated pseudotime in effectively tracking the maturation process of NK cells.

Through these analyses, we identified functional clusters and revealed the existence of multiple subsets of NK cells within the lung tissue, undergoing a well-defined maturation process, as previously described in other compartments, such as the blood and spleen.

Impaired maturation process of NK cells in the tumor microenvironment results in the exclusion of cytotoxic NK cells

To investigate the maturation process of intratumoral NK cells during tumor progression, we compared the expression of genes involved in NK maturation in small and large tumors and non-tumoral lung tissues over the pseudotime (**Figure 4A**). While the gene expression patterns of each maturation phase were comparable in small tumors and in non-tumoral tissues (except for *Ets1)*, we found that the maturation process was strongly impaired in large tumors, since the majority of the genes involved in NK cell maturation displayed altered patterns. Specifically, the expression of early differentiation genes was sustained for a longer duration over the pseudotime, and the expression of late maturation genes did not persist until the end of the maturation process. According to the previously identified role of IL-15 as a key cytokine involved in NK cell maturation, we observed decreased expression of *Il15ra* in intratumoral NK cells compared to that in non-tumoral lungs (**Figure S4C**).

To determine the functional consequences of altered maturation of intratumoral NK cells, we analyzed the proportion of each NK cell cluster and found that large tumors were enriched in cytokine-producing NK cell clusters (**Figure 4B**). Subsequently, we quantified each NK cell subset based on CD27 and CD11b expression by flow cytometry (a representative image of flow cytometry is shown in **Figure S6A**). In line with Figure 1E, all subsets exhibited a decrease in absolute numbers in tumoral samples compared with non-tumoral lungs (**Figure S6B**). However, the proportion of $CD27^{-}CD11b^{+}$ cytotoxic NK cells was reduced in tumor samples, whereas that of $CD27^{+}CD11b^{-}$ cytokine-producing NK cells was slightly higher in small tumors

than in non-tumoral lungs, confirming the single-cell sequencing results (**Figure 4C**). In conclusion, our findings indicate impaired NK cell maturation within the TME, resulting in a substantial tumor-size-dependent decrease of cytotoxic NK cells.

Increased NK cell death and impaired cytotoxic function of NK cells in the TME

In addition to altered NK cell maturation towards cytotoxic phenotypes, we investigated the intratumoral NK cell death. We found a higher number of dead NK cells in large tumors than in small tumors and non-tumoral tissues **(Figure 5A)**. This increase was predominantly attributed to an increased death of mature $CD27^{+}CD11b^{+}$ and $CD27^{-}CD11b^{+}$ NK cells **(Figure 5B)**. To further decipher the mechanisms underlying NK cell death within the TME, we quantified a panel of cytokines and FasL in the supernatant of non-tumoral, small, and large tumors. We observed a substantial increase, ranging from 3 to 127-fold, in the levels of IL-1α, IL-1β, IL-2, IL-6, IL-15, IL-23, CCL2, IFN-β, IFN-γ, TGF-β, and TNF-α, in large compared to small tumors or non-tumoral tissues (**Figure 5C**). The only exception was the decrease in IL-17A levels in the large tumor supernatant. We also identified a tumor-specific secretion of soluble FasL, exhibiting a 5.6-fold increase in large tumors compared to that in small tumors, with a significant overexpression of the *Fas*-encoding gene in NK cells from large tumors compared to non-tumoral tissue and small tumors (**Figure S6C**). Interestingly, at protein level, this increased expression of Fas was only observed on the surface of $CD27^{-}CD11b^{+}$ cytotoxic NK cells in large tumors (**Figure S6D**). These results suggest that the mature cytotoxic NK cells are going apoptosis following tumor killing. Consistent with this hypothesis, we found that some NK cells are localized close to cleaved-caspase 3 expressing tumor cells, and interestingly that some of these NK cells are positive for cleaved-caspase 3 marker (**Figure 5D**). We also found a positive correlation between Fas and CD107 expression by NK cells (**Figure S6E**).

Finally, we investigated the cytotoxic function of $CD27^{-}CD11b^{+}$ NK cells, by analyzing the capacity of cytotoxic NK cells to lyse LLC tumor cells upon activation. NK cells from small tumors exhibited a 10% increase in their ability to lyse tumor cells, whereas NK cells from large tumors showed an 8% decrease compared to their non-tumoral counterparts (**Figure 5E**). Altogether, these findings suggest an increased NK cell death in large tumors, that could be mediated by FAS-FASL. Simultaneously, the cytotoxic capabilities of the remaining $CD27^{-}$ $CD11b^{+}$ NK cells are impaired, diminishing their ability to lyse tumor cells.

Tumor stage-dependent impaired NK cell maturation in human lung tumors results in reduced proportion of cytotoxic NK cells

Finally, to determine whether NK cell maturation is also altered in human tumors, we analyzed a publicly available single-cell transcriptomic dataset comprising 47 NSCLC samples and their non-tumoral counterparts[17]. We first performed RNA-seq-based clustering and identified more than 50 immune clusters (**Figure S7A**). Next, we specifically focused on NK cells, characterized by the expression of *NCR1*, *NCAM1*, *KLRD1*, *KLRF1*, *GNLY*, *NKG7*, *SPON2*, *PRF1*, *GZMB* and *FCGR3A* and the absence of *CD3D*, *CD3E*, *CD8A*, *TRAC*, *EPCAM*, *MARCO* and *CD19* expression. We generated a UMAP comprising 1314 NK cells and identified 10 clusters (**Figure 6A**). We subsequently characterized these clusters, revealing that clusters 3, 7 and 9 correspond to cytokine-producing NK cells, while clusters 0, 1, 2, 4, 5, 6 and 8 correspond to cytotoxic cells, as revealed by the bubble plot and gene enrichment analyses **(Figure 6B, Figure S7B)**. Notably, the IL-17 and TNF signaling pathways, Th1/Th2 differentiation and NF-kB activation pathways were upregulated in clusters 3, 7 and 9. Conversely, NK cell mediated cytotoxicity pathways were downregulated in these clusters. The classification of NK cell populations was further confirmed using MiloR package as we did for murine NK cells (**Figure S7C**). Strikingly, the proportions of each cluster varied between non-tumoral tissues and

different tumor stages, with an over-representation of clusters 3, 7 and 9 and an under-representation of clusters 0, 1, 2, 4, 5, 6 and 8 in stages II and III tumors **(Figure 6C, Figure S7D).**

To investigate the maturation process of NK cells within the human lung TME, we conducted a pseudotime analysis to identify a NK cell developmental trajectory **(Figure 6D)**. This trajectory was validated by analyzing the concurrent expression of 13 genes associated with cytokine-producing NK cells **(Figure S7E, upper panel)** and 22 associated with cytotoxic NK cells **(Figure S7E, lower panel)**[7]. As expected, genes linked to cytokine-producing NK cells were expressed at the early pseudotime points (pseudotimes 0 to 7), preceding the expression of genes linked to cytotoxic NK cells (pseudotimes 10 to 15). Consistent with our findings in murine tumors, we observed a profound impairment in the maturation process of intratumoral NK cells in a tumor-stage dependent manner **(Figure 6E)**. Specifically, while the gene expression profile over the pseudotime was quite similar between stage I tumors and non-tumoral tissues, it became increasingly disrupted in stage II and even more in stage III tumors. This outcome reinforces the notion that impaired NK cell maturation within the TME leads to a reduced population of cytotoxic NK cells.

We also noted the expression of *FAS* in NK cell clusters, with higher expression observed in cytotoxic NK cells than in cytokine producers **(Figure 6G)**. Importantly, *FASLG* was expressed by specific clusters of immune CD3-expressing T-cells within the lung TME **(Figure 6H)**. Considering immune checkpoint molecules, we found a significant higher expression of *LAG3, TIGIT, CTLA4*, and *PDCD1*, and a decrease in the expression of *LAMP1* in NK cells from tumor tissues than in non-tumoral tissues **(Figure S7F)**. The expression of *GZMB* and *PRF1* was also reduced in NK cells, depending on the tumor-stage (**Figure S7G).**

We validated these findings at protein level in an additional cohort of 30 NSCLC patients, conducting a phenotypic analysis of intratumoral NK cells. We categorized patients in an unsupervised manner based on the intratumoral NK cell phenotype (**Figure 6I).** We identified four distinct groups characterized by decreased expression of CD16, DNAM-1, NKp80 and NKp30 (from group 1 to 4). Upon comparing the tumor size across these groups, a discernible trend emerged, reaching statistical significance and indicating an increase in tumor size from groups 1 to 4 (**Figure 6J**). Collectively, these results highlight the specific exclusion of cytotoxic NK cells from the TME, where they exhibit an altered phenotype, particularly in large tumors.

Discussion

NK cells are often both scarce and functionally compromised within the TME of various solid tumors, including lung cancer[5,18–20]. In the present study, we investigated the tumor-stage dependent characteristics of intratumoral NK cells using an orthotopic lung cancer model. We first characterized the phenotype of intratumoral NK1.1^{+} CD3^{-} cells and found that the majority were NK cells (CD49a^{+}, CD49b^{-}), with less than 10% identified as ILC1-like cells (CD49a^{+}, CD49b^{+}) and 2% as ILC1 cells (CD49a^{-}, CD49b^{+}). The presence of ILC1-like cells may indicate a conversion of NK cells into ILC1s, as previously observed in the study by Gao *et al*., which demonstrated a TGF-β-dependent conversion of NK cells into ILC1-like and ILC1s within the TME[28]. In our tumor model, intratumoral NK cells did not express immune checkpoint molecules, with the exception of LAG-3, and exhibited reduced cytotoxic activity in large tumors. These findings are consistent with the studies which reported that intratumoral murine NK cells lack PD-1 expression[29], while they may express LAG3[30].

We observed a reduction in NK cell numbers, impaired maturation process and diminished cytotoxic functions, depending on the tumor progression. These results highlight the relevance of this model, which closely mirrors the progressive exclusion of NK cells observed in human lung tumors[18]. Furthermore, our results align with recent reports indicating that NK cells become dysfunctional immediately upon entering the TME[31]. Consequently, the NK cell depletion did not influence tumor progression, as demonstrated in our study.

Pseudotime analysis revealed a profound impairment in the NK cell maturation process, particularly in advanced tumor stages. This impairment leads to the accumulation of cytokine-producing NK cell subsets and a diminished generation of fully mature cytotoxic NK cells. The cytokine-producing NK cells are primarily characterized by increased expression of the TNF-α signaling pathway, IFN-γ response, IL-2 signaling, IFN-α response, and TGF-β signaling.

However, since these cells do not express IL-10 immunosuppressive cytokine transcripts, they were not classified as regulatory NK cells. These findings are consistent with the observations of Jin *et al*.[32], where a notable abundance of $CD11b^{-}CD27^{-}$ NK cells, exhibiting an immature and inactive phenotype, was observed within human NSCLC. The authors concluded that the heightened proportion of the double-negative population correlated with tumor stage and tumor size and significantly influenced the clinical outcomes of the patients. Among the cytokines having an important role in NK cell biology, IL-15 is required for NK cell maturation[9]. In line with this, our study identifies a diminished IL15RA expression by NK cells from large murine tumors, potentially explaining the impaired maturation process of NK cells in this context, despite the increased concentration of IL-15 that was quantified in the tumor supernatant of large tumors.

We present compelling evidence that defective NK cell maturation contributes to the emergence of less cytotoxic NK cell subsets, which was observed across various tumor types[33]. Additionally, these NK cells showed increased susceptibility to cell death. In large tumors, we observed robust FasL secretion and gene expression of FasL in $CD3^{+}$ T cells, alongside elevated Fas expression in intratumoral NK cells. In contrast, we did not detect FasL transcripts in regulatory T cells or Fas expression in LLC cells. These findings suggest that NK cell death may be mediated by Fas-FasL interactions, with FasL expressed by T cells and Fas by NK cells. However, to further elucidate the mechanisms and cell types involved in NK cell killing, additional experiments are needed to characterize FasL-expressing cells in the TME and to investigate the molecular pathways responsible for increased FasL secretion. Supporting our observations, increased Fas expression has been reported in NK cells from gastric cancer patients, correlating with higher apoptosis rate[34]. Similarly, Poggi *et al*.[35] demonstrated that engagement of natural cytotoxic receptors (NCRs:NKp30, NKp44 and NKp46) induces FasL up-

regulation in NK cells, with melanoma cells promoting NK cell death via NCR Fas-FasL interaction. *In vivo* mechanistic studies are required to further validate the involvement of Fas-FasL in NK cell death, such as blocking the interaction using monoclonal antibodies against Fas or FasL. In vitro, we could not reproduce increased NK cell death by incubating murine lung NK cells with supernatants from large tumors, highlighting the need for formal confirmation of Fas-FasL involvement. Notably, we found a correlation between Fas and CD107 expression in NK cells, suggesting that activated NK cells may be prone to cell death. This is consistent with reports showing that NK cells are susceptible to apoptosis due to TRAIL expression, and that cytokines such as TNF-α enhance Fas expression[36]. Additionally, the lung TME is known to be hypoxic, with HIF-1α being a key transcription factor in response to hypoxia[37]. It has been shown that under hypoxic conditions, NK cells exhibit reduced proliferation and are functionally impaired[38]. However, a direct link between hypoxia and NK cell death has yet to be established and warrants further investigation.

In the complex TME of NSCLC, several factors may contribute to the scarcity of intratumoral NK cells. A recent study implicated TREM-2 expressing monocytes-derived macrophages in the dysfunction and paucity of these NK cells[39]. Therefore, it is crucial to conduct further investigations that comprehensively explore the interactions between immune cell densities and phenotypes within the TME, including the roles of Fas, FasL, and cytokine secretion, across different tumor stages. Such coordinated efforts will improve our understanding of the mechanisms driving NK cell dysfunction and scarcity in NSCLC, potentially uncovering additional therapeutic avenues.

Altogether, our findings suggest that the prevalence of non-cytotoxic NK cells in the TME results from multiple tumor-size-dependent escape mechanisms. Various factors within the TME of large tumors may hinder NK cell effector functions and block their maturation. The

cytokine profile related to advanced tumor stages could account for the impaired maturation of NK cells. In this study, we observed increased cytokine secretion in large tumors, including inflammatory cytokines and TGF-β, with the latter playing a key role in NK cell dysfunction[40]. Additional studies are needed to confirm the involvement of these cytokines or to identify other soluble factors in the TME that contribute to impaired NK cell maturation and function. Furthermore, our study opens avenues for human translation, as the maturation stages of NK cells in mice and humans show substantial similarities in both genetic signatures and functional properties[7]. Although the precise mechanisms behind the toxicity of tumor supernatant on single positive $CD11b^+$ NK cells remain unclear, we hypothesize that similar dynamics may occur in human tumors.

Several NK cell-based therapeutic strategies are currently being developed for solid tumors. While promising, their efficacy is often limited by NK cell resistance mechanisms and their low abundance within tumors[41–43]. This study underscores the importance of advancing our understanding of NK cell biology within the TME. Such insights are critical for optimizing NK-based therapies, with the dual goals of protecting these cells from cell death and enhancing their cytotoxic functions.

Limitations of study

Our study has several limitations, including (a) the fact that we were not able to sort a high number of NK cells because they are scarce in the large tumors, (b) we could not reproduce the induction of NK cell death *in vitro* in a coculture assay with lung tumor cell lines, probably because the induction of NK cell death in the tumor microenvironment depends on multiple factors, and the tumor cells do not secrete Fas-L *in vitro,* (c) we could not reproduce the induction of NK cell death and Fas induction on NK cells when NK cells were incubated *in vitro* with supernatant from large tumors, (d) the impact of the tumor microenvironment on NK cell death and maturation process cannot be addressed mechanistically *in vitro* since many cells of the tumor microenvironment do not survive after resection from mice and dilaceration.

Author contributions

JR, CT, SM, NM, EV, and NJ performed the experiments. JR, DS, MM, IH, and PEF performed the bioinformatic analysis. JR, CT, NM and IC analyzed the data. IC designed and supervised the study. JR, and IC wrote the manuscript. SS, NB, PEJ and DD revised the manuscript.

Acknowledgements

This study was supported by Institut National de la Sante et de la Recherche Medicale (INSERM), Sorbonne Universite, Labex Immuno-oncology and Institut National du cancer (PL-BIO).

We thank the Center of Histology Imaging and Cytometry (CHIC) and the Centre d'Exploration Fonctionnelle (CEF) facilities of the Centre de Recherche des Cordeliers. We also thank Cochin hospital for the single-cell RNA-seq experiment. Finally, we thank Bertrand Escalière and Yann Kerdiles (Centre d'Immunologie de Marseille-Luminy) for their help regarding the pseudotime analysis.

Declaration of interests

The authors have declared that no conflict of interest exists.

Figure titles and legends

Figure 1

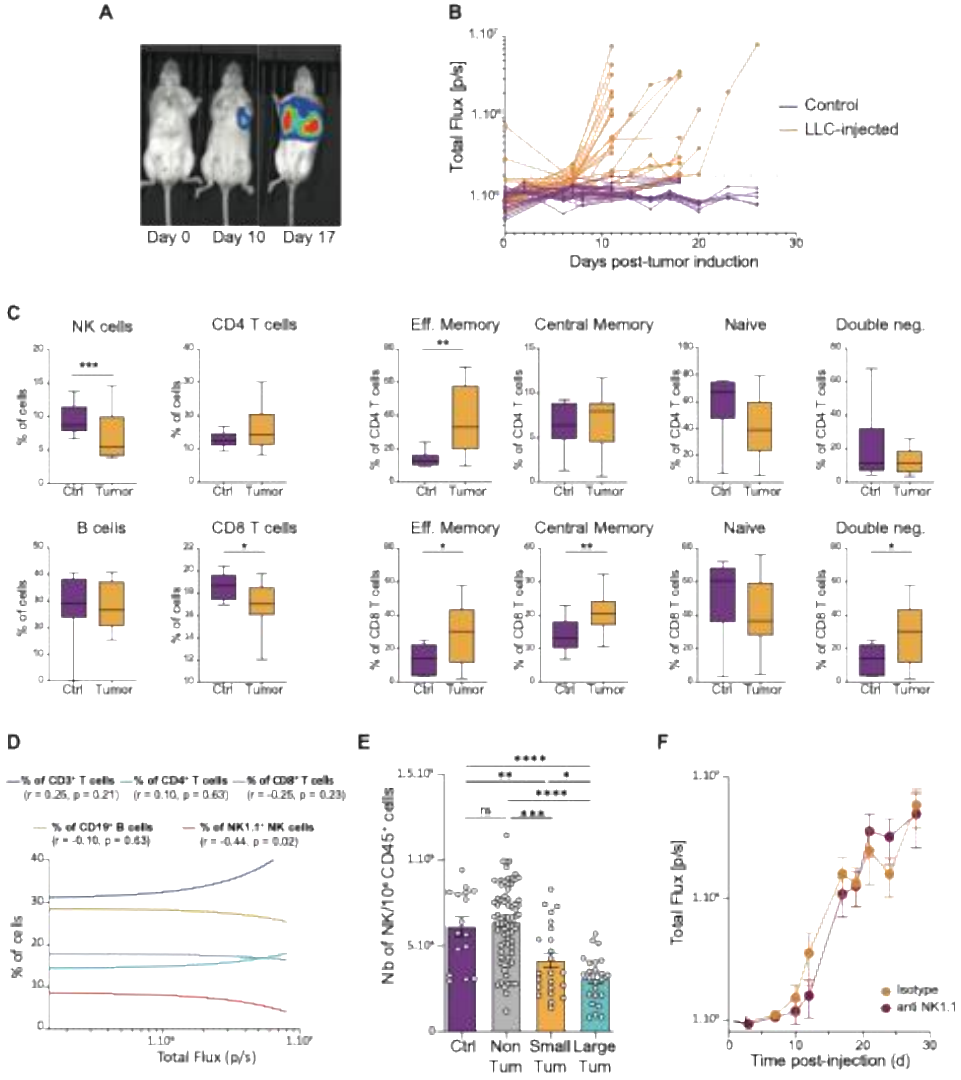

Figure 1. NK cell exclusion from the TME depends on the tumor progression. (A) Detection of chemiluminescence in the lungs of C57/Bl6 albino mice that were intratracheally injected with luciferase-expressing LLC cells. The bioluminescent signal, allowing a follow-up of the tumor growth, was captured at days 0 (day of injection), 10 and 17. **(B)** Follow-up of the tumor growth in Control (injected with culture medium, purple curves) and LLC-injected mice (orange curves). The size of the tumor is expressed as total flux (p/s), which is calculated by defining the same region of interest (ROI) for each mouse independently, as a function of time.

Background has been set-up at 2.10^5 p/s (dotted line). **(C)** Boxplots of the proportion of NK cells, B cells, and CD4 and CD8 T cells (left), as well as effector memory ($CD62L^-CD44^+$), central memory ($CD62L^+CD44^+$), naïve ($CD62L^+CD44^+$), and double negative ($CD62L^-CD44^-$) $CD4^+$ and $CD8^+$ T cell subsets (right) in control and tumoral lungs. Error bars represent mean ± SEM. Statistical comparisons were performed using unpaired (Mann-Whitney) t-test. *: p≤0.05; **: p≤0.01; ***: p≤0.001. **(D)** Correlations between each immune lymphoid population and the tumor size. For each curve, the Spearman coefficient and the p-value are indicated. **(E)** Number of NK cells per million of $CD45^+$ cells in control (Ctrl), non-tumoral (Non Tum) or tumoral lungs with small (Small Tum) or large (Large Tum) tumors. Two independent experiments were performed with a total of 34-36 mice each. Error bars represent mean ± SEM. Statistical analyses were performed using unpaired (Mann-Whitney) or paired (Wilcoxon) t-tests according to matched samples or not. *: p≤0.05; **: p≤0.01; ***: p≤0.001; ****: p≤0.0001. **(F)** Follow-up of the tumor growth in mice injected with control isotype (Isotype) or with anti-NK1.1 antibody to deplete NK cells (anti-NK1.1). Error bars represent mean ± SEM and each condition contains 8 or 9 mice, depending on the experimental group.

Figure 2.

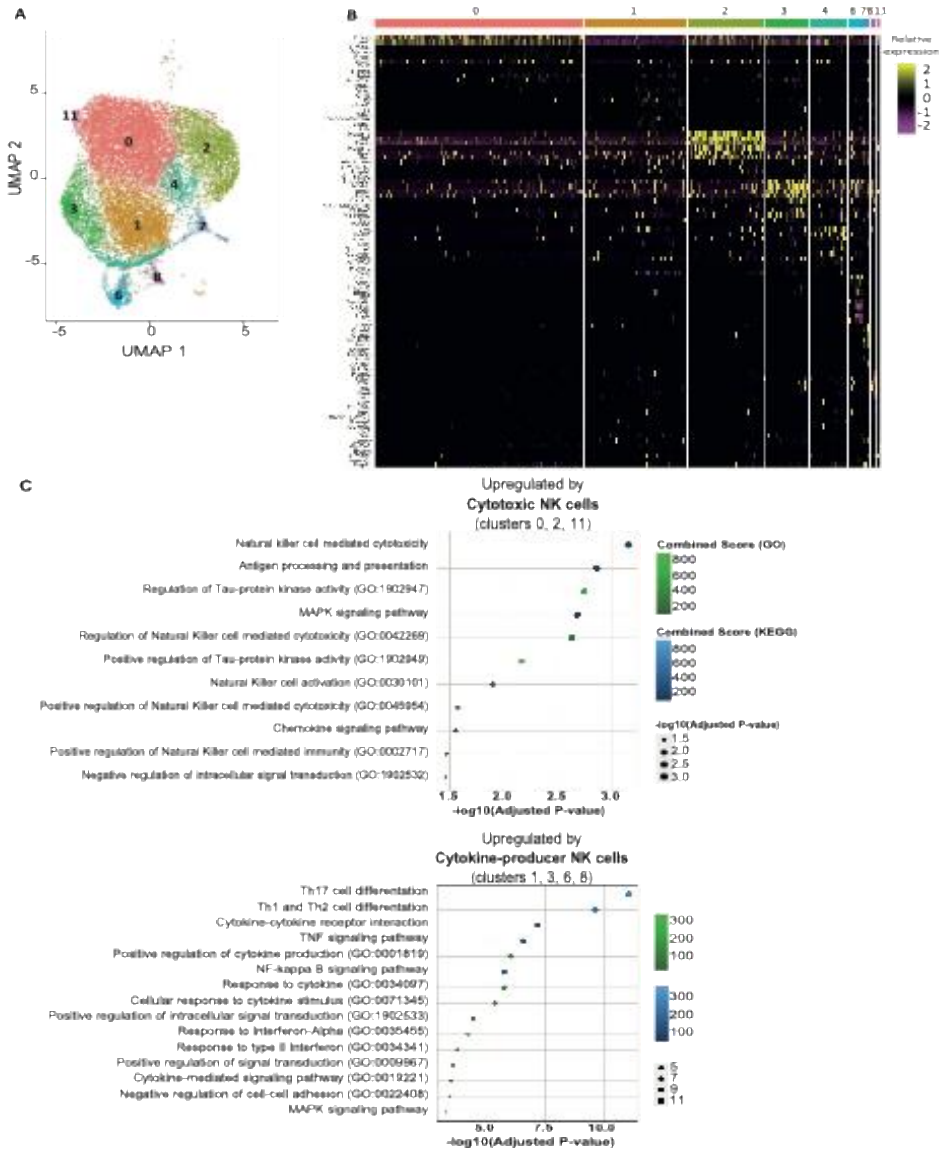

Figure 2. Cytotoxic and cytokine-producer subsets of intratumoral NK cells are identified in the TME. (A) UMAP displaying NK cell clusters generated from single-cell analysis of sorted NK cells. **(B)** Heatmap representation of the top 10 differentially expressed genes for each cluster. Identification of differentially expressed genes has been achieved using the MAST method. **(C)** Pathways up-regulated by the cluster 0 (upper bubble plot) and cluster 6 (lower bubble plot) which are representative of the cytotoxic (0, 2 and 11) and cytokine-producer (1, 3, 6 and 8) NK cell clusters, respectively. The bubble plots show the significant most relevant enriched

signatures to immune cell functions from the Kyoto Encyclopedia of Genes and Genome (KEGG) and Gene Ontology Biological process (GO) databases. Signatures are ordered according to adjusted p-values, the color graduation shows the overlap between the datasets signature and our own signature.

Figure 3.

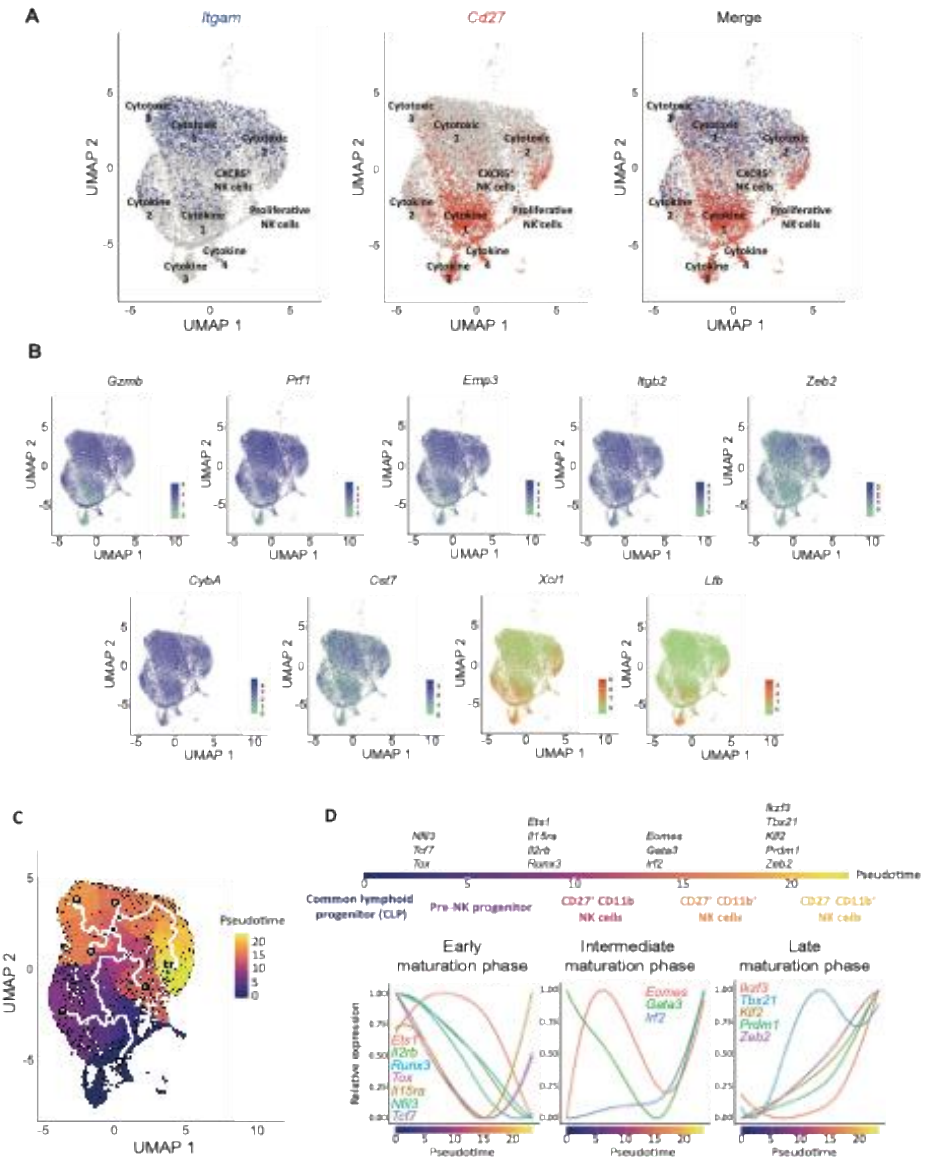

Figure 3. Maturation stages of intratumoral NK cells, from cytokine-producer to cytotoxic subsets. (A) UMAP representations of CD11b-encoding gene (*Itgam*), CD27-encoding gene

(*Cd27*) and merged expression. **(B)** UMAP representations of *Gzmb*, *Prf1*, *Emp3*, *Itgb2*, *Zeb2*, *CybA*, *Cst7*, *Xcl1* and *Ltb* gene expression by cytotoxic (green to blue scale) and cytokine-producer (green to red scale) NK cell clusters. **(C)** UMAP showing the pseudotime path across the single-cell generated clusters. **(D)** Genes implicated at every stage of NK cell maturation in mice (top) and their relative expression across the pseudotime in all samples (bottom).

Figure 4

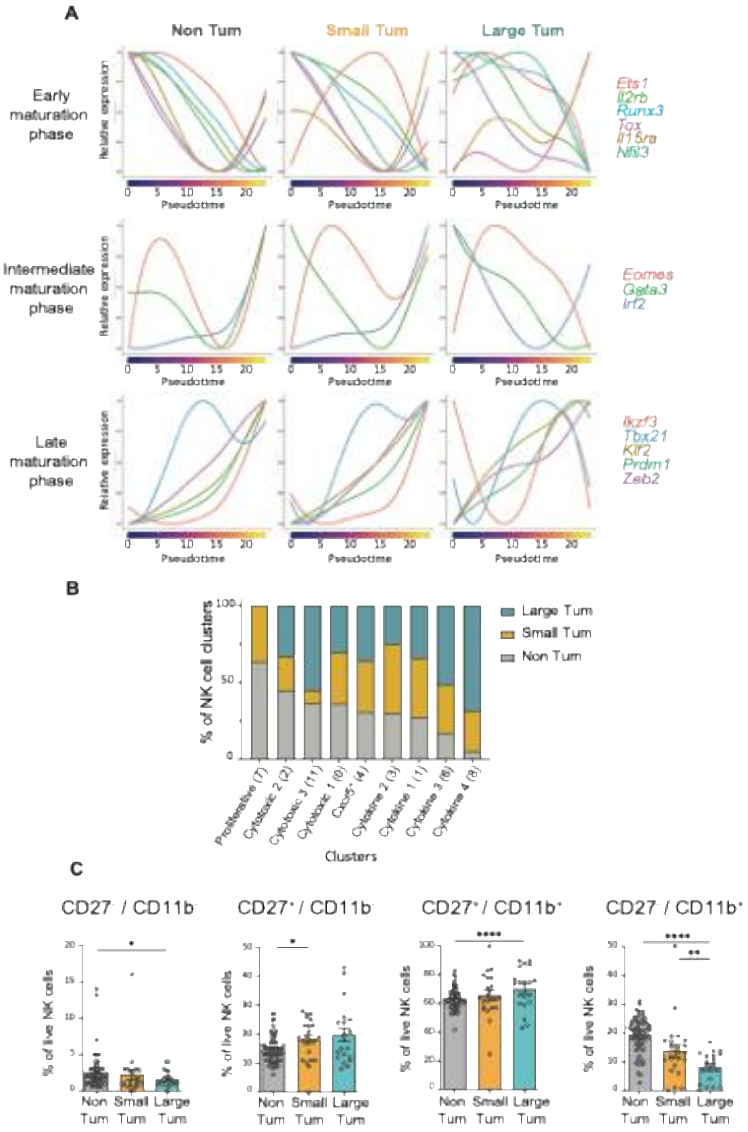

Figure 4. Impaired maturation process of NK cells in the tumor microenvironment results in the exclusion of cytotoxic NK cells. (A) Relative expression of genes implicated in early (*Ets1,*

Il2rb, Runx3, Tox, Il15ra and *Nfil3* - top), intermediate (*Eomes*, *Gata3,* and *Irf2* - middle) and late (I*kzf3, Tbx21, Klf2, Prdm1* and *Zeb2* - bottom) maturation stages across the pseudotime. Samples are divided into non-tumoral ("Non Tum." - left), small ("Small Tum." - center) and large ("Large Tum." - right) tumors. **(B)** Percentage of NK cell clusters in non-tumoral lungs, and in small and large tumors. The clusters are ordered from the higher to lower percentage in non-tumoral samples. The number of each cluster is indicated in brackets. **(C)** Quantification of live NK cell subsets in the three groups of mice and in every subset of NK cells. Error bars represent mean ± SEM. Statistical analyses were performed using unpaired (Mann-Whitney) or paired (Wilcoxon) t-tests according to matched samples or not. *: p≤0.05; **: p≤0.01; ****: p≤0.0001.

Figure 5

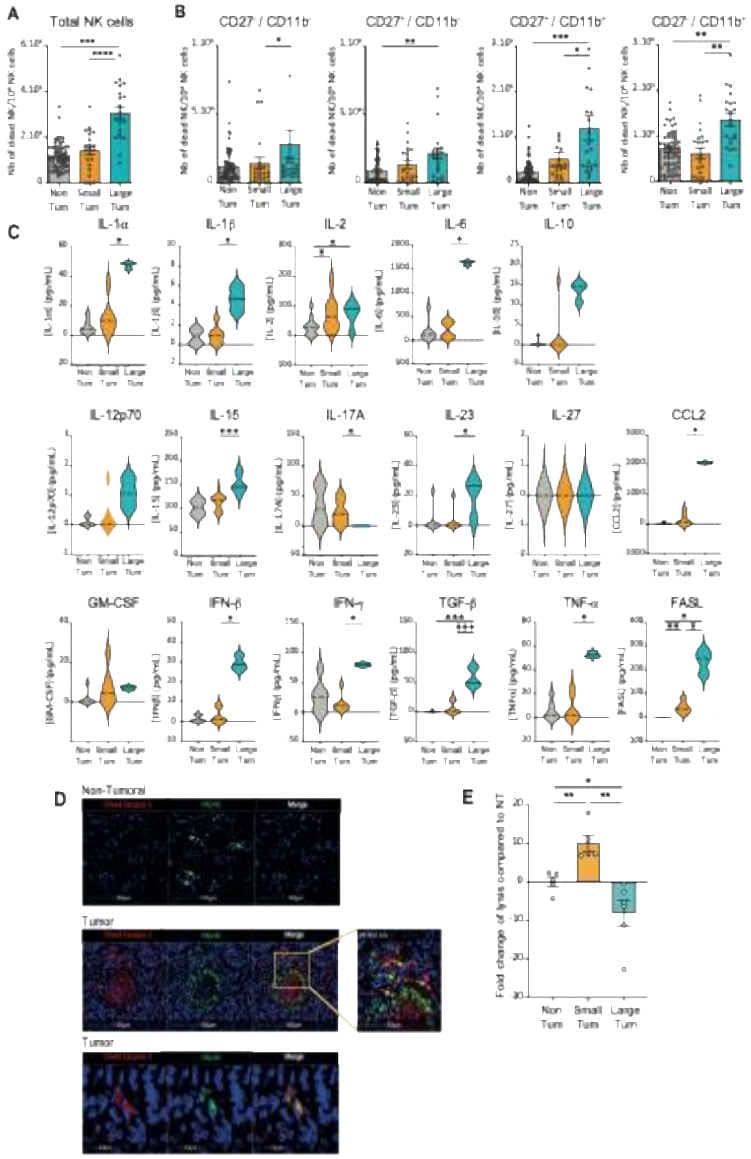

Figure 5. Increased NK cell death and impaired cytotoxic functions of NK cells in the TME

(A) Number of dead total NK cells or **(B)** segregated by subset, in non-tumoral lung (Non Tum), small (Small Tum) and large (Large Tum) tumors. **(C)** Concentration of cytokines and FasL in the supernatant of non-tumoral lung (Non Tum), small (Small Tum) and large (Large Tum) tumors. **(D)** Detection of NKp46^{+} NK cells and cleaved caspase 3 in non-tumoral lung and in tumors, by immunofluorescence. Green arrows indicate NKp46^{+} cells and yellow arrows show cells that co-express NKp46 and cleaved-caspase 3. **(E)** Percentage of LLC cell lysis by the

cytotoxic subset of NK cells ($CD27^{-}CD11b^{+}$) purified from non-tumoral (Non Tum), small (Small Tum), or large tumors (Large tum). The percentages of lysis have been normalized to the non-tumoral condition. Error bars represent mean ± SEM. Statistical analyses were performed using unpaired (Mann-Whitney) or paired (Wilcoxon) t-tests according to matched samples or not. *: p≤0.05; **: p≤0.01. ***: p≤0.001; ****: p≤0.0001.

Figure 6

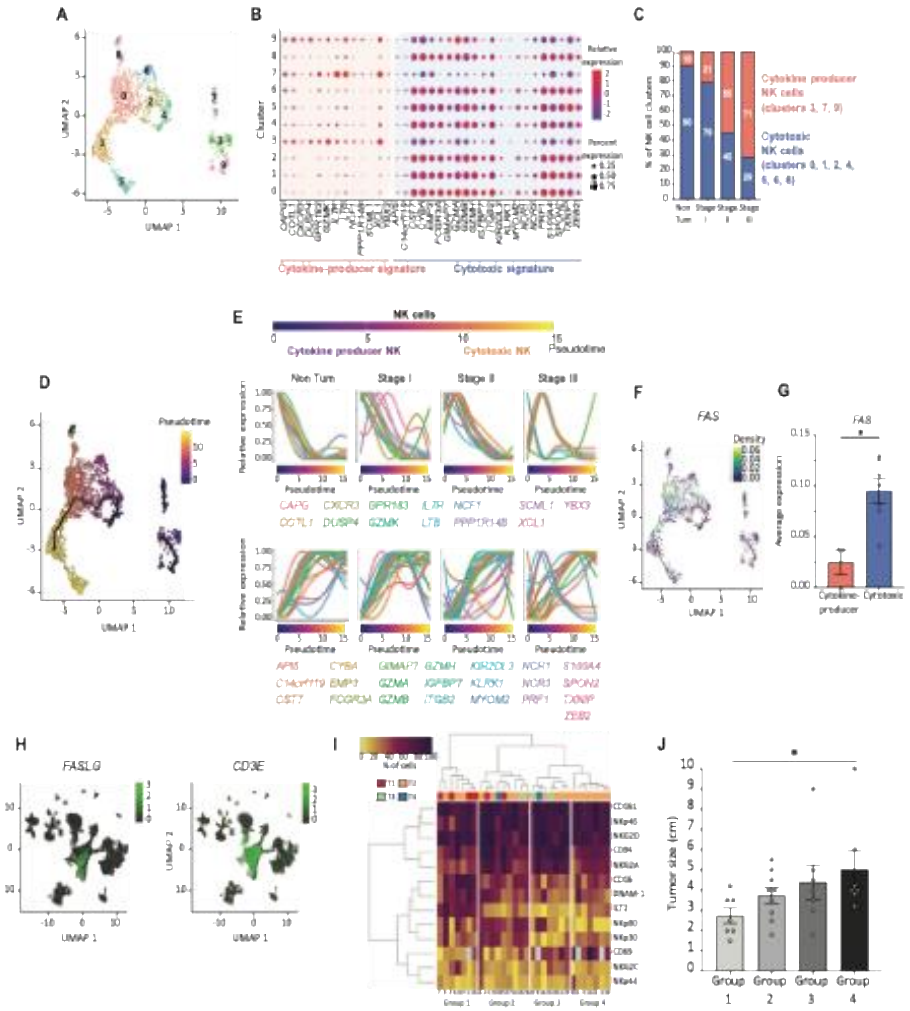

Figure 6. Impaired NK cell maturation in human tumors results in a decreased number of cytotoxic NK cells. (A) UMAP of NK cells clusters generated from Leader et al. [17]. **(B)** Bubble plot representing the gene expression of cytokine-producer (left) or cytotoxic (right) NK cell

signature in every cluster. **(C)** Percentage of cytotoxic (blue) or cytokine-producer (red) clusters in every tumor stage. **(D)** UMAP showing the pseudotime path across the generated clusters. **(E)** Representation of human NK cell maturation across the generated pseudotime (top), and relative expression of cytokine-producers (middle) and cytotoxic (bottom) signatures over the pseudotime across non-tumoral (Non Tum), Stage I, II and III tumoral samples. **(F)** UMAP representation of *FAS* gene expression by NK cell clusters. **(G)** Quantification of *FAS* expression by cytokine-producer (red) and cytotoxic (blue) clusters. **(H)** UMAP representation of *FASLG* and *CD3E* gene expression by all the immune cells analyzed in Leader *et al.* [17]. **(I)** Heatmap showing the phenotype of intratumoral NK cells in the NSCLC cohort. Each row represents a marker and each column represents a patient. Groups 1 to 4 have been defined according to the dendrogram clustering tree. TNM stage (from T1 to T4) is indicated on top of the heatmap. **(J)** Tumor size in the four groups of patients. Error bars represent mean ± SEM. Statistical analyses were performed by the Mann-Whitney test. *: $p \leq 0.05$.

Tables

Table 1: Top 10 genes expressed by each NK cell cluster as compared to the other clusters, with the lowest adjusted p-value (< 10^{-6})

Cluster 0	Cluster 1	Cluster 2	Cluster 3	Cluster 4	Cluster 6	Cluster 7	Cluster 8	Cluster 11
Emb	Emb	Crem	Gadd45b	Nme1	Il7r	Pclaf	Rsad2	Eef1a1
Xcl1	Cd27	Hspa1b	Nfkbia	Ppp1r14b	Tmem176b	Mki67	Slfn5	Actb
Hsp90ab1	Ctla2a	Jun	Nfkbid	Nme2	Tcrg-C4	Clspn	Ifi204	Ppia
Hspa8	Ly6c2	Txnip	Pim1	Srm	Gpr183	Spc24	Ifit3	H2afz
Gzma	Gzmb	Hspa1a	Icam1	Mettl1	Krt83	Birc5	Ifi44	Ptma
Ly6e	Tnfsf8	Klf2	Nfkbiz	C1qbp	Gzma	Uhrf1	Rtp4	Fth1
Ccr2	Ccr2	Klf6	Kdm6b	Hsp90ab1	Inpp4b	Stmn1	Ifit1	S100a10
Tnfsf8	Eef1a1	Ccl3	Bcl2a1b	Ptma	Ramp1	Cdk1	Bst2	Rack1
Dok3	Rassf9	Ncr1	Rel	Npm1	Prf1	E2f1	Sox17	Actg1
Ctla2a	Tppp3	Rhob	Bcl2a1d	Fbl	Cntn1	Cks1b	P4ha2	Ftl1

STAR METHODS

REAGENT or RESOURCE	SOURCE	IDENTIFIER
Antibodies		
Live/Dead Fixable Yellow Dead Cell Stain Kit	ThermoFischer	L34959
CD3 - APC eF780	eBiosciences	47-0033-82
CD3 - AF 700	BD PharMingen	557984
CD3 - FITC	BD PharMingen	553062
CD4 - PE-Texas Red	Invitrogen	MCD0417
CD8 - FITC	BD PharMingen	553031
CD11b - BV785	Biolegend	101243
CD11b - FITC	eBiosciences	553310
CD19 - APC Cy7	BD Biosciences	557655
CD27 - APC	eBiosciences	17-0271-82
CD44 - APC eF780	eBiosciences	47-0441-82
CD45 - Pe Cy7	BD PharMingen	552848
CD62L - APC	BD PharMingen	553152
CD107a - BV421	Biolegend	12-16-17
CD107a - PerCP-eF710	Invitrogen	46-1071-82
CTLA-4 - BV605	BioLegend	106323
CX3CR1 - BV786	BioLegend	49029
CXCR5 - PE-eF610	eBiosciences	61-7185-82
CXCR6 - BV421	BioLegend	151109
Fas - PE	BD ParMingen	15405B
LAG-3 - eF450	Invitrogen	48-2231-82
NK1.1 - APC vio770	Miltenyi	130-118-686
NK1.1 - BV605	BD PharMingen	563220
PD-1 - PerCP-eF710	Invitrogen	46-9985-82
S1PR1 - PE	R&D Systems	FAB7089P
TIGIT - BV650	BD Biosciences	744213
TIM-3 - PE	eBiosciences	12-5871-82

Anti-NK1.1 mAb	BioXcell	BX-BE0036
IgG2a isotype control	BioXcell	BX-BE0085
Bacterial and virus strains		
Biological samples		
Human primary lung tumors (Non-Small Cell Carcinoma, NSCLC)	Cochin hospital	With patient's consent and agreement of the French ethic committee
Chemicals, peptides, and recombinant proteins		
Dulbecco's modified Eagle's medium (DMEM)	Gibco	41965-039
Fetal calf serum (FCS)	Eurobio	CVFSVF0101
Penicillin-streptomycin	Gibco	15140-122
Hygromycin B	Gibco	10687010
Ketamine hydrochloride	Virbac	Ketamine hydrochloride
Xylazine hydrochloride	Elanco	Xylazine hydrochloride
XenoLight D-Luciferin-K^+ Salt	PerkinElmer	122799
Isofluorane	Perkin Elmer	Isofluorane
EDTA	Invitrogen	AM9262
Hematoxylin	Dako	53309
Eosin	Abcam	ab246824
Recombinant Murine IL-2	Peprotech	212-12
Recombinant Murine IL-15	Peprotech	210-15
CFSE	Invitrogen	C34554
Critical commercial assays		
Mycoplasma Detection Kit	Ozyme	LT07-710
Tumor Dissociation Kit	Miltenyi	130-096-730
Chromium Next GEM Single Cell 3' GEM, Library & Gel Bead Kit v3.1	10X Genomics	Chromium Next GEM Single Cell 3'
Quantikine Mouse Fas Ligand/TNFSF6 kit	R&D System	MFL00
LEGENDplex Multi-Analyte Flow Assay kit	BioLegend	LEGENDplex
Deposited data		
Leader_et_al dataset	www.github.com/effiken/Leader_et_al	
Experimental models: Cell lines		
luciferase-expressing Lewis Lung Carcinoma (LLC-luc) cells	ATCC	CRL-1642
Experimental models: Organisms/strains		
Albino B6(C)/Rj-Tyrc/c mice	Janvier Labs	Albino B6(C)/Rj-Tyrc/c
Oligonucleotides		

Recombinant DNA		
Software and algorithms		
Living image system	Perkin Elmer	
FlowJo software	BD Biosciences	
Halo software	Indica Labs	
Diva software	BD Biosciences	
Rstudio software		version 4.2.2
Seurat package		version 5.0.1
EnrichR package		version 3.2
Monocle 3 package		version 1.3.1
MiloR package		version 1.6.0
MiloDE package		Version 0.0.0.9000
LEGENDplex v8 software	BioLegend	
Other		
PBS	Gibco	14190-094
RPMI 1640 medium	Gibco	R7388
Transwell plates	VWR	89235-020

Resource availability

Lead contact

Further information and requests for resources and reagents should be directed to Isabelle Cremer (isabelle.cremer@sorbonne-universite.fr).

Materials availability

This study did not generate novel reagents

Data and code availability

- The single cell sequencing data generated in this study are available at the Gene Expression Omnibus, accession number: GSE278856.
- The original code is accessible at the following link: https://github.com/JulesRussick/Tumor-stage-driven-disruption-of-NK-cell-maturation-and-cytotoxic-functions-in-the-lung-TME
- Any additional information required to reanalyze the data reported in this work paper is available from the lead contact upon request."

Experimental model and study participant details

Cell cultures – LLC Luciferase

The luciferase-expressing Lewis Lung Carcinoma (LLC-luc) cells (ATCC, CRL-1642) were obtained from Vincenzo di Bartoo in 2015 (Institut Pasteur, France) and were cultured in Dulbecco's modified Eagle's medium (DMEM, Gibco, 41965-039) containing 10% fetal calf serum (FCS) (Eurobio, CVFSVF0101), 1% penicillin-streptomycin (Gibco, 15140-122) and 1% hygromycin B (Gibco, 10687010). The cells were not cultured for more than 15 passages. All cell lines were routinely tested for Mycoplasma with a kit (Ozyme, LT07-710). No specific authentication of the cell lines was performed.

Orthotopic tumor induction in mice

Albino B6(C)/Rj-Tyrc/c mice (Janvier Labs, Le Genest-Saint-Isle, France) (6-8 weeks old, females) were anesthetized using 100 mg/kg of Ketamine hydrochloride (Virbac, Centravet, France) and 10 mg/kg of Xylazine hydrochloride (Elanco, Centravet, France) (100µL/mice). After 12 minutes at room temperature, $0.3x10^6$ LLC-Luc were injected with a cannula into the trachea in 30 µL of medium culture. The mice were placed on top of a heat plate until their waking up and put back in the cage. The weight of mice was controlled every 2-3 days after tumor injection, and tumor progression was measured every 2-3 days by bioluminescence using IVIS Lumina II Imaging system. Mice were injected intraperitoneally with D-Luciferin (XenoLight D-Luciferin-K+ Salt, PerkinElmer, 122799; 150 mg Luciferin/kg body weight). Ten minutes after D-Luciferin injection, the bioluminescent signal was acquired using the IVIS Lumina II system (Perkin Elmer, Waltham, MA, USA). During the acquisition procedure, mice were anesthetized with 2.5% Isofluorane (XGI-8 Gas anesthesia system, Perkin Elmer), for 10 minutes. Data were analyzed with Living image software by defining a region of interest on the thoracic area of each mouse and extracting the corresponding total flux. All mice were

maintained in ventilated cages and housed in specific pathogen free conditions in full accordance with FELASA recommendations. The project received approval from the Charles Darwin Ethics Committee for animal experimentation (APAFIS 22332-2019100811051145) and by the French Ministry of Agriculture (Paris, France).

NSCLC patients – In-house cohort

Human primary lung tumors from 30 NSCLC were obtained from Cochin hospital (Paris) the day of surgery, with patient's consent and agreement of the French ethic committee (number 2012 06 12 IRB00001072) in application with the article L. 1121-1 of French law, according to the recommendations in the Helsinki declaration. None of the patients received neo-adjuvant chemotherapy or radiotherapy. The inclusion criteria are histological subtypes squamous cell carcinoma (SCC) or lung adenocarcinoma (ADC), all TNM stages, and associated with clinical data. Histopathologic features such as histological subtypes, ADC grade, TNM stages are available for the majority of the patients. We categorized patients in an unsupervised manner based on the intratumoral NK cell phenotype**.** Analysis of sex-based differences was not performed due to sample size.

Method details

Preparation of lung murine single-cell suspension

Lungs of euthanized mice were flushed with 10mL of PBS (Gibco, 14190-094) to remove blood. Non-tumoral parts of the lung were then separated from the tumoral ones (with IVIS verification) and harvested in RPMI 1640 medium (Gibco) in gentleMacs C tubes (Miltenyi). Single-cell suspensions were obtained after enzymatic disruption using the Tumor Dissociation Kit (Miltenyi, 130-096-730) in the gentleMACS Octo Dissociator (program "mouse tumor dissociation kit - 37°C") at 37°C and filtered through a 70 µm cell strainer (Falcon, 352350).

Cells were washed in PBS + 5% FCS + 0.5mM EDTA (Invitrogen, AM9262), and the number of cells obtained was determined by manual counting on Kova slides (Kova, 87144).

Flow cytometry

Cell suspensions were incubated in the corresponding antibody mix, in PBS + 10% FCS medium, for 30' at 4°C. The list of monoclonal antibodies used are listed in the Supplementary Table 1. After a wash in PBS + 5% FCS + 0.5mM EDTA, cells were resuspended in 300µL of PBS + 10% FCS medium. Stainings were acquired on Fortessa X20 (BD Biosciences) and analyzed using FlowJo software (BD Biosciences).

In vivo NK cell depletion

Mice were intratracheally injected as described above and the tumor growth was followed 3 times per week. As soon as the total flux reached 2.105 p/s, mice were injected intraperitoneally with either 400µg of anti-NK1.1 mAb (PK136 - BioXcell, BX-BE0036) or the control isotype (IgG2a - BioXcell, BX-BE0085) in 200 µL of PBS with insulin syringe (Dutscher, 324891). The depletion was then maintained each week by IP injection of 200µg of antibody or isotype. Additionally, blood was collected to control the depletion by flow cytometry.

Detection of tumors by Hematoxylin and Eosin staining

The mice underwent intracardiac perfusion with PBS and 4% paraformaldehyde before dissection. Lung tissue was embedded in paraffin using Leica ASP300/Histocore Arcadia H instrument and 3-5 µm sections were cut. Slides were deparaffinized and rehydrated and incubated for 3 minutes in Hematoxylin solution (Dako, 53309). After 3 washes in water, of 3 minutes each, slides were incubated for 30 seconds in Eosin solution (Abcam, ab246824; H&E). Finally, slides were mounted using Glycergel Mounting Medium (Dako). Slides were scanned using Axioscan scanner (Zeiss) and acquisitions were done with Halo software (Indica Labs).

NK cell sorting

Cells from single-cell suspension were stained as mentioned in Flow cytometry section and resuspended at 7.106 cells/mL. The sorting was performed using a fluorescence activated cell sorting (FACS) Aria III cell sorter (BD Biosciences), using 100µm noodle. Sorted NK cells were defined as Live/Dead-, CD45+, CD3-, NK1.1+ and CD11b and CD27 markers were added to sort NK cell subsets. Purity after sorting was analyzed by flow cytometry using Diva software (BD Biosciences).

Single-cell library preparation and sequencing

After cell sorting, NK cells from each sample were subjected to Chromium Next GEM Single Cell 3' GEM, Library & Gel Bead Kit v3.1 (10X Genomics, Pleasanton, California, USA), following the Chromium Single Cell 3 Reagent Kits v3.1 protocol targeting 10,000 cells per condition. Briefly, Single-cell Gel Bead-In-Emulsions (GEMs) were generated in oil droplets with barcoded beads using a Chromium Controller instrument (10X Genomics). cDNA was generated in each droplet, purified using DynaBeads MyOne Silane Beads and amplified by PCR (11 cycles) using reagents from the kit. Fragments size estimation of the amplified cDNA was assessed using SPRIselect Reagent Kit and fragmented with High SensitivityTM HS DNA kit on 2100 Bioanalyzer (Agilent) and quantified using QubitTM dsDNA High Sensitivity HS assay (ThermoFisher Scientific). Libraries were then sequenced with HighOutput flowcell using an Illumina Nextseq500.

Single cell analysis

Single cell analyses were performed using Rstudio software version 4.2.2, with the Seurat package version 5.0.1[44] and using MiloR package, version 1.6.0[24] and MiloDE package, version 0.0.0.9000[25]. Nodes were generated using MiloR package. After annotating the cells, values of

k were set to 50 and 10 for mouse and human analysis, respectively. The chosen reduction methods were the same as for the Seurat analysis. The analysis of the differentially expressed genes were done using MiloDE package. Only genes with a "pval_corrected_across_genes" <0.05 were considered as significant.

Murine single-cell analysis

Data filtering and normalization: For the subsequent analysis, only cells exhibiting less than 5% of mitochondrial gene content and a gene count ranging from 200 to 3000 were retained. Additionally, ribosomal genes were excluded from the analysis. Normalization was performed using the "LogNormalize method" (natural-log transformation using log1p) through Seurat's "NormalizeData" function. The relative expression of each gene was centered using the Seurat "ScaleData" method and linear dimensional reduction was conducted with the Seurat "RunPCA" function.

Clustering and identification of cluster signatures: Clustering was achieved using the Seurat "FindClusters" function (with resolution = 0.5) employing the Louvain algorithm. Marker genes for each cluster were defined as differentially expressed genes within the cluster in comparison to all other cells. This was accomplished using the Seurat "FindMarkers" function, with the following parameters: test.use = MAST, logfc.threshold = 0.25 and min.pct = 0.1.

Gene Enrichment analysis: Enrichment analysis was conducted using the EnrichR package, version 3.2[45–47]. Biological processes and pathways were assessed using the "KEGG 2019 Mouse'' and "Gene Ontology Biological Process 2023" signatures. Only signatures with significant q-values ≤0.05 were considered relevant.

Human single-cell analysis

Data filtering and normalization: The processed dataset, formatted as an R object was downloaded from www.github.com/effiken/Leader_et_al. Data were then normalized using the "LogNormalize method" (natural-log transformation using log1p) of the Seurat "NormalizeData" function. The relative expression of each gene was centered using Seurat "ScaleData", followed by linear dimensional reduction performed with the Seurat "RunPCA" function.

Clustering and identification of NK cell cluster signatures: Clustering was achieved using the Seurat "FindClusters" function, employing the Louvain algorithm. To accurately identify NK cells within the dataset, three consecutive runs were performed. Each run involved clustering the cells, assessing gene expression in each cluster, excluding non-NK cell clusters and then clustering the remaining cells. NK cells were defined as *CD3D*$^{-}$, *CD3E*$^{-}$, *CD8A*$^{-}$, *CD19*$^{-}$, *EPCAM*$^{-}$, *MARCO*$^{-}$, *TRAC*$^{-}$, *GNLY*$^{+}$, *KLRD1*$^{+}$, *NCR1*$^{+}$, *NKG7*$^{+}$, *FCGR3A*$^{+/-}$, *GZMB*$^{+/-}$, *KLRF1*$^{+/-}$, *NCAM1*$^{+/-}$, *PRF1*$^{+/-}$, *SPON2*$^{+/-}$.

Following the identification and clustering of (resolution = 1), marker genes for each cluster were determined as differentially expressed genes within that specific cluster compared to all other cells. It was accomplished using the Seurat "FindMarkers" function with the following parameters: test.use = MAST, logfc.threshold = 0.5 and min.pct = 0.5.

Gene Enrichment analysis: Gene enrichment analysis was performed using the EnrichR package, version 3.2. For biological processes and pathways, the "KEGG 2021 Human'' and "Gene Ontology Biological Process 2023" signatures were used. Only significant signatures with q-values ≤0.05 were considered relevant.

Pseudotime analysis

Pseudotime analysis was performed using the Monocle 3 package, version 1.3.1[26]. The initial point representing the most immature NK cells was chosen based on low expression of *Itgam* in mice and high expression of *NCAM1* high with low expression of *FCGR3A* in humans.

Tumor supernatant preparation

The tumor supernatants for NK cells culture experiment, obtained from tumor cell suspension (small and large tumors), were centrifuged and filtered on 0.22µm cell strainer (Millipore, SLGV033RS), and conserved at -80°C until use. The same procedure was done to obtain supernatants from wild-type lungs of albinos C57/Bl6 mice, as controls.

Fas Ligand and cytokine quantification

Quantification of mouse FasL, IL-2, IL-15 and TGF-β was performed by ELISA using the Quantikine Mouse Fas Ligand/TNFSF6 kit, mouse TGF-β1 DuoSet, mouse IL-15 DuoSet and mouse IL-2 kit (R&D System, MFL00, DY1679, DY447 and M2000, respectively), according to the manufacturer's instructions. Other cytokine production was assessed using the LEGENDplex Multi-Analyte Flow Assay kit (BioLegend, San Diego, CA), allowing the simultaneous quantification of 13 cytokines (IL1-α, IL1-β, IL-6, IL-10, IL-12p70, IL-17A, IL-23, IL-27, GM-CSF, IFN-β, IFN-γ, CCL2 and TNF). The results were analyzed with the LEGENDplex v8 software (BioLegend).

Immunofluorescence

Mice were intracardiacally perfused with PBS and 4% paraformaldehyde before dissection. Lung tissue was embedded in paraffin using Leica ASP300/Histocore Arcadia H instrument and 3-5 µm sections were cut. Slides were introduced in a PT-Link instrument (Dako) pre-warmed at 99 °C for 30 min at pH 9. After washing in TBS-Tween 0.04%, endogenous peroxidase was inactivated, and lung tissues were placed into a blocking solution (protein block (Dako, X0909), BSA 5%, Triton 0.1%) for 15 min. Then, anti-NKp46 antibody (R&D system, ref AF2225, 1/1000

diluted in blocking buffer) was added for 15 min at RT followed by the polymer ImmPRESS anti-goat HRP (Vector lab, MP7405) for 10 min and Opal 690 (Akoya, FP1497001KT) at 1/200 for 10 min. Then slides were warmed at 99°C 10 min at pH4. After washing, slides were blocked into the blocking buffer at pH6 and anti-cleaved caspase 3 antibody was added for 20 min at 1/500 into the blocking buffer (Cell Signaling, 9664L) followed by Opal polymer Ms+Rb (Akoya, ARH1001EA) and Opal 570 added at 1/200 (Akoya, FP1488001KT) for 10 min. All sections were stained with DAPI (1 µg/mL, Invitrogen, D1306) for 5 min and mounted in Prolong Diamond anti-fade mounting (Invitrogen, P36961). Slides were scanned using Axioscan (Zeiss) and acquisitions were done with Halo software (Indica Labs).

Cytotoxicity assay

NK cell subsets were sorted from lungs of tumor-bearing mice as described above, resuspended in RPMI 1640 containing 5% Penicillin-Streptomycin, 10% FCS, IL-2 (200 UI/mL), and IL-15 (50 ng/µL) (Peprotech, 212-12 and 210-15) and deposited in 96 well plates. In parallel, LLC tumor cells were stained with CFSE (Invitrogen, C34554) for 20 minutes. After three washes, LLC cells were incubated with NK cells at 1:1 ratio for 3h. Detection of lysed cells was achieved by CFSE staining by flow cytometry.

Hierarchical clustering

Hierarchical clustering was performed using the “as.dendrogram” function which uses the Ward D2 method.

Quantification and statistical analysis

Tests used for comparisons are indicated in the corresponding figure legends. For most statistical analysis, unpaired (Mann-Whitney) or paired (Wilcoxon) t-tests were used according to matched samples or not. Samples coming from the same animal (non-tumoral vs corresponding tumoral) were considered paired, while samples coming from different animals

were considered unpaired. Error bars represent mean ± SEM. Spearman's rank test was used for all correlations. GraphPad Prism was used to determine p-values. p-values of less than 0.05 were considered significant. *: p≤0.05; **: p≤0.01; ***: p≤0.001; ****: p≤0.0001.

Additional resources

Public dataset of NSCLC patients from Leader et al.: www.github.com/effiken/Leader_et_al

References

1. Altorki, N.K., Markowitz, G.J., Gao, D., Port, J.L., Saxena, A., Stiles, B., McGraw, T., and Mittal, V. (2019). The lung microenvironment: an important regulator of tumour growth and metastasis. Nat Rev Cancer *19*, 9–31. https://doi.org/10.1038/s41568-018-0081-9.

2. Vivier, E., Tomasello, E., Baratin, M., Walzer, T., and Ugolini, S. (2008). Functions of natural killer cells. Nat Immunol *9*, 503–510. https://doi.org/10.1038/ni1582.

3. Melaiu, O., Lucarini, V., Cifaldi, L., and Fruci, D. (2020). Influence of the Tumor Microenvironment on NK Cell Function in Solid Tumors. Front. Immunol. *10*, 3038. https://doi.org/10.3389/fimmu.2019.03038.

4. Vivier, E., Artis, D., Colonna, M., Diefenbach, A., Di Santo, J.P., Eberl, G., Koyasu, S., Locksley, R.M., McKenzie, A.N.J., Mebius, R.E., et al. (2018). Innate Lymphoid Cells: 10 Years On. Cell *174*, 1054–1066. https://doi.org/10.1016/j.cell.2018.07.017.

5. Russick, J., Torset, C., Hemery, E., and Cremer, I. (2020). NK cells in the tumor microenvironment: Prognostic and theranostic impact. Recent advances and trends. Seminars in Immunology *48*, 101407. https://doi.org/10.1016/j.smim.2020.101407.

6. Zhang, C., and Tian, Z. (2017). NK cell subsets in autoimmune diseases. Journal of Autoimmunity *83*, 22–30. https://doi.org/10.1016/j.jaut.2017.02.005.

7. Crinier, A., Milpied, P., Escalière, B., Piperoglou, C., Galluso, J., Balsamo, A., Spinelli, L., Cervera-Marzal, I., Ebbo, M., Girard-Madoux, M., et al. (2018). High-Dimensional Single-Cell Analysis Identifies Organ-Specific Signatures and Conserved NK Cell Subsets in Humans and Mice. Immunity *49*, 971-986.e5. https://doi.org/10.1016/j.immuni.2018.09.009.

8. Marquardt, N., Kekäläinen, E., Chen, P., Lourda, M., Wilson, J.N., Scharenberg, M., Bergman, P., Al-Ameri, M., Hård, J., Mold, J.E., et al. (2019). Unique transcriptional and protein-expression signature in human lung tissue-resident NK cells. Nat Commun *10*, 3841. https://doi.org/10.1038/s41467-019-11632-9.

9. Bi, J., and Wang, X. (2020). Molecular Regulation of NK Cell Maturation. Front. Immunol. *11*, 1945. https://doi.org/10.3389/fimmu.2020.01945.

10. Held, W., Jeevan-Raj, B., and Charmoy, M. (2018). Transcriptional regulation of murine natural killer cell development, differentiation and maturation. Cell. Mol. Life Sci. *75*, 3371–3379. https://doi.org/10.1007/s00018-018-2865-1.

11. Chiossone, L., Chaix, J., Fuseri, N., Roth, C., Vivier, E., and Walzer, T. (2009). Maturation of mouse NK cells is a 4-stage developmental program. Blood *113*, 5488–5496. https://doi.org/10.1182/blood-2008-10-187179.

12. Hayakawa, Y., and Smyth, M.J. (2006). CD27 Dissects Mature NK Cells into Two Subsets with Distinct Responsiveness and Migratory Capacity. J Immunol *176*, 1517–1524. https://doi.org/10.4049/jimmunol.176.3.1517.

13. Kim, S., Iizuka, K., Kang, H.-S.P., Dokun, A., French, A.R., Greco, S., and Yokoyama, W.M. (2002). In vivo developmental stages in murine natural killer cell maturation. Nat Immunol *3*, 523–528. https://doi.org/10.1038/ni796.

14. Delahaye, N.F., Rusakiewicz, S., Martins, I., Ménard, C., Roux, S., Lyonnet, L., Paul, P., Sarabi, M., Chaput, N., Semeraro, M., et al. (2011). Alternatively spliced NKp30 isoforms affect the prognosis of gastrointestinal stromal tumors. Nat Med *17*, 700–707. https://doi.org/10.1038/nm.2366.

15. Gillard-Bocquet, M., Caer, C., Cagnard, N., Crozet, L., Perez, M., Fridman, W.H., Sautès-Fridman, C., and Cremer, I. (2013). Lung Tumor Microenvironment Induces Specific Gene Expression Signature in Intratumoral NK Cells. Frontiers in Immunology *4*. https://doi.org/10.3389/fimmu.2013.00019.

16. Halama, N., Braun, M., Kahlert, C., Spille, A., Quack, C., Rahbari, N., Koch, M., Weitz, J., Kloor, M., Zoernig, I., et al. (2011). Natural Killer Cells are Scarce in Colorectal Carcinoma Tissue Despite High Levels of Chemokines and Cytokines. Clin Cancer Res *17*, 678–689. https://doi.org/10.1158/1078-0432.CCR-10-2173.

17. Leader, A.M., Grout, J.A., Maier, B.B., Nabet, B.Y., Park, M.D., Tabachnikova, A., Chang, C., Walker, L., Lansky, A., Le Berichel, J., et al. (2021). Single-cell analysis of human non-small cell lung cancer lesions refines tumor classification and patient stratification. Cancer Cell *39*, 1594-1609.e12. https://doi.org/10.1016/j.ccell.2021.10.009.

18. Platonova, S., Cherfils-Vicini, J., Damotte, D., Crozet, L., Vieillard, V., Validire, P., Andre, P., Dieu-Nosjean, M.-C., Alifano, M., Regnard, J.-F., et al. (2011). Profound Coordinated Alterations of Intratumoral NK Cell Phenotype and Function in Lung Carcinoma. Cancer Research *71*, 5412–5422. https://doi.org/10.1158/0008-5472.CAN-10-4179.

19. Russick, J., Joubert, P.-E., Gillard-Bocquet, M., Torset, C., Meylan, M., Petitprez, F., Dragon-Durey, M.-A., Marmier, S., Varthaman, A., Josseaume, N., et al. (2020). Natural killer cells in the human lung tumor microenvironment display immune inhibitory functions. J Immunother Cancer *8*, e001054. https://doi.org/10.1136/jitc-2020-001054.

20. Stankovic, B., Bjørhovde, H.A.K., Skarshaug, R., Aamodt, H., Frafjord, A., Müller, E., Hammarström, C., Beraki, K., Bækkevold, E.S., Woldbæk, P.R., et al. (2018). Immune Cell Composition in Human Non-small Cell Lung Cancer. Front Immunol *9*, 3101. https://doi.org/10.3389/fimmu.2018.03101.

21. Cong, J., Wang, X., Zheng, X., Wang, D., Fu, B., Sun, R., Tian, Z., and Wei, H. (2018). Dysfunction of Natural Killer Cells by FBP1-Induced Inhibition of Glycolysis during Lung Cancer Progression. Cell Metab. *28*, 243-255.e5. https://doi.org/10.1016/j.cmet.2018.06.021.

22. Peng, L., Zhang, J., Teng, Y., Zhao, Y., Wang, T., Mao, F., Lv, Y., Cheng, P., Li, W., Chen, N., et al. (2017). Tumor-Associated Monocytes/Macrophages Impair NK-Cell Function via TGFβ1 in Human Gastric Cancer. Cancer Immunology Research *5*, 248–256. https://doi.org/10.1158/2326-6066.CIR-16-0152.

23. Finak, G., McDavid, A., Yajima, M., Deng, J., Gersuk, V., Shalek, A.K., Slichter, C.K., Miller, H.W., McElrath, M.J., Prlic, M., et al. (2015). MAST: a flexible statistical framework for assessing transcriptional changes and characterizing heterogeneity in single-cell RNA sequencing data. Genome Biol *16*, 278. https://doi.org/10.1186/s13059-015-0844-5.

24. Dann, E., Henderson, N.C., Teichmann, S.A., Morgan, M.D., and Marioni, J.C. (2022). Differential abundance testing on single-cell data using k-nearest neighbor graphs. Nat Biotechnol *40*, 245–253. https://doi.org/10.1038/s41587-021-01033-z.

25. Missarova, A., Dann, E., Rosen, L., Satija, R., and Marioni, J. (2024). Leveraging neighborhood representations of single-cell data to achieve sensitive DE testing with miloDE. Genome Biol *25*, 189. https://doi.org/10.1186/s13059-024-03334-3.

26. Trapnell, C., Cacchiarelli, D., Grimsby, J., Pokharel, P., Li, S., Morse, M., Lennon, N.J., Livak, K.J., Mikkelsen, T.S., and Rinn, J.L. (2014). The dynamics and regulators of cell fate decisions are revealed by pseudotemporal ordering of single cells. Nat Biotechnol *32*, 381–386. https://doi.org/10.1038/nbt.2859.

27. Qi, J., Crinier, A., Escalière, B., Ye, Y., Wang, Z., Zhang, T., Batista, L., Liu, H., Hong, L., Wu, N., et al. (2021). Single-cell transcriptomic landscape reveals tumor specific innate lymphoid cells associated with colorectal cancer progression. Cell Rep Med *2*, 100353. https://doi.org/10.1016/j.xcrm.2021.100353.

28. Gao, Y., Souza-Fonseca-Guimaraes, F., Bald, T., Ng, S.S., Young, A., Ngiow, S.F., Rautela, J., Straube, J., Waddell, N., Blake, S.J., et al. (2017). Tumor immunoevasion by the conversion of effector NK cells into type 1 innate lymphoid cells. Nat Immunol *18*, 1004–1015. https://doi.org/10.1038/ni.3800.

29. Judge, S.J., Dunai, C., Aguilar, E.G., Vick, S.C., Sturgill, I.R., Khuat, L.T., Stoffel, K.M., Van Dyke, J., Longo, D.L., Darrow, M.A., et al. (2020). Minimal PD-1 expression in mouse and human NK cells under diverse conditions. J Clin Invest *130*, 3051–3068. https://doi.org/10.1172/JCI133353.

30. Gemelli, M., Noonan, D.M., Carlini, V., Pelosi, G., Barberis, M., Ricotta, R., and Albini, A. (2022). Overcoming Resistance to Checkpoint Inhibitors: Natural Killer Cells in Non-Small Cell Lung Cancer. Front Oncol *12*, 886440. https://doi.org/10.3389/fonc.2022.886440.

31. Dean, I., Lee, C.Y.C., Tuong, Z.K., Li, Z., Tibbitt, C.A., Willis, C., Gaspal, F., Kennedy, B.C., Matei-Rascu, V., Fiancette, R., et al. (2024). Rapid functional impairment of natural killer cells following tumor entry limits anti-tumor immunity. Nat Commun *15*, 683. https://doi.org/10.1038/s41467-024-44789-z.

32. Jin, J., Fu, B., Mei, X., Yue, T., Sun, R., Tian, Z., and Wei, H. (2013). CD11b−CD27− NK Cells Are Associated with the Progression of Lung Carcinoma. PLoS ONE *8*, e61024. https://doi.org/10.1371/journal.pone.0061024.

33. Portale, F., and Di Mitri, D. (2023). NK Cells in Cancer: Mechanisms of Dysfunction and Therapeutic Potential. IJMS *24*, 9521. https://doi.org/10.3390/ijms24119521.

34. Saito, H., Takaya, S., Osaki, T., and Ikeguchi, M. (2013). Increased apoptosis and elevated Fas expression in circulating natural killer cells in gastric cancer patients. Gastric Cancer *16*, 473–479. https://doi.org/10.1007/s10120-012-0210-1.

35. Poggi, A., Massaro, A.-M., Negrini, S., Contini, P., and Zocchi, M.R. (2005). Tumor-Induced Apoptosis of Human IL-2-Activated NK Cells: Role of Natural Cytotoxicity Receptors. The Journal of Immunology *174*, 2653–2660. https://doi.org/10.4049/jimmunol.174.5.2653.

36. Mikhailova, V.A., Sokolov, D.I., Grebenkina, P.V., Bazhenov, D.O., Nikolaenkov, I.P., Kogan, I.Y., and Totolian, A.A. (2024). Apoptotic Receptors and CD107a Expression by NK Cells in an Interaction Model with Trophoblast Cells. Curr Issues Mol Biol *46*, 8945–8957. https://doi.org/10.3390/cimb46080528.

37. Ziółkowska-Suchanek, I. (2021). Mimicking Tumor Hypoxia in Non-Small Cell Lung Cancer Employing Three-Dimensional In Vitro Models. Cells *10*, 141. https://doi.org/10.3390/cells10010141.

38. Garcés-Lázaro, I., Kotzur, R., Cerwenka, A., and Mandelboim, O. (2022). NK Cells Under Hypoxia: The Two Faces of Vascularization in Tumor and Pregnancy. Front Immunol *13*, 924775. https://doi.org/10.3389/fimmu.2022.924775.

39. Park, M.D., Reyes-Torres, I., LeBerichel, J., Hamon, P., LaMarche, N.M., Hegde, S., Belabed, M., Troncoso, L., Grout, J.A., Magen, A., et al. (2023). TREM2 macrophages drive NK cell paucity and dysfunction in lung cancer. Nat Immunol *24*, 792–801. https://doi.org/10.1038/s41590-023-01475-4.

40. Viel, S., Marçais, A., Guimaraes, F.S.-F., Loftus, R., Rabilloud, J., Grau, M., Degouve, S., Djebali, S., Sanlaville, A., Charrier, E., et al. (2016). TGF-β inhibits the activation and functions of NK cells by repressing the mTOR pathway. Sci Signal *9*, ra19. https://doi.org/10.1126/scisignal.aad1884.

41. Murray, S., and Lundqvist, A. (2016). Targeting the tumor microenvironment to improve natural killer cell-based immunotherapies: On being in the right place at the right time, with resilience. Human Vaccines & Immunotherapeutics *12*, 607–611. https://doi.org/10.1080/21645515.2015.1096458.

42. Nayyar, G., Chu, Y., and Cairo, M.S. (2019). Overcoming Resistance to Natural Killer Cell Based Immunotherapies for Solid Tumors. Front Oncol *9*. https://doi.org/10.3389/fonc.2019.00051.

43. Bald, T., Krummel, M.F., Smyth, M.J., and Barry, K.C. (2020). The NK cell–cancer cycle: advances and new challenges in NK cell–based immunotherapies. Nat Immunol *21*, 835–847. https://doi.org/10.1038/s41590-020-0728-z.

44. Butler, A., Hoffman, P., Smibert, P., Papalexi, E., and Satija, R. (2018). Integrating single-cell transcriptomic data across different conditions, technologies, and species. Nat Biotechnol *36*, 411–420. https://doi.org/10.1038/nbt.4096.

45. Chen, E.Y., Tan, C.M., Kou, Y., Duan, Q., Wang, Z., Meirelles, G.V., Clark, N.R., and Ma'ayan, A. (2013). Enrichr: interactive and collaborative HTML5 gene list enrichment analysis tool. BMC Bioinformatics *14*, 128. https://doi.org/10.1186/1471-2105-14-128.

46. Kuleshov, M.V., Jones, M.R., Rouillard, A.D., Fernandez, N.F., Duan, Q., Wang, Z., Koplev, S., Jenkins, S.L., Jagodnik, K.M., Lachmann, A., et al. (2016). Enrichr: a comprehensive gene set enrichment analysis web server 2016 update. Nucleic Acids Res *44*, W90–W97. https://doi.org/10.1093/nar/gkw377.

47. Xie, Z., Bailey, A., Kuleshov, M.V., Clarke, D.J.B., Evangelista, J.E., Jenkins, S.L., Lachmann, A., Wojciechowicz, M.L., Kropiwnicki, E., Jagodnik, K.M., et al. (2021). Gene Set Knowledge Discovery with Enrichr. Current Protocols *1*, e90. https://doi.org/10.1002/cpz1.90.